3-D Joint Inversion of Gravity and Magnetic Data Using Data-Space and Truncated Gauss–Newton Methods

Rongzhe Zhang, Tonglin Li, Cai Liu, Xingguo Huang, Kristian Jensen, and Malte Sommer

***Abstract*— Gravity and magnetic inversion are important methods for comprehensive quantitative interpretation of data obtained in, e.g., mineral, oil and gas, and geothermal exploration. At present, the 3-D joint inversion technology of gravity and magnetic data is facing challenges from large-scale data exploration applications. In this letter, a new algorithm for 3-D joint inversion of gravity and magnetic data with high accuracy and low computational cost is presented. We use the geometric trellis method to perform fast forward calculations and then introduce the sparse constraint and adaptive sensitivity matrix into the model constraint terms. The inexact structural resemblance method is then used to add the cross-gradient constraint penalty term to the objective function. Finally, an algorithm (DS-TGN) combining data-space (DS) and truncated Gauss–Newton (TGN) methods is used to solve the joint inversion objective function. Numerical experiments with synthetic data show that the proposed algorithm can significantly reduce the computational cost and obtain high accuracy density and magnetization models with structural resemblance and sharp boundaries. We also apply the DS-TGN algorithm to data obtained in the area of Greater Khingan in northwestern Heilongjiang, China. The underground density and magnetization distribution results provide a high-resolution geological model for the detection of skarn-type deposits.**

***Index Terms*— Cross gradient, data space (DS), gravity method, joint inversion, magnetic method, truncated Gauss–Newton (TGN).**

I. Introduction

GEOPHYSICAL inversion refers to inferring the spatial distribution of subsurface properties from geophysical data. This may provide information on the physical and elastic properties of the subsurface, as well as the geometric shapes of geological targets of interest. However, uncertainties and nonuniqueness are common in geophysical inversion results [1]. To reduce the ambiguity of the inversion results and obtain more accurate information of the subsurface properties, different types of regularization methods or *a priori* information [2]–[5] can be used.

With the maturity of separate inversion technology and the complexity of the exploration environment, the idea of joint inversion of integrated geophysical data has attracted widespread attention [6]–[10]. For the joint inversion of different geophysical datasets, the most important issue is how to couple model parameters. Currently, there are two general joint inversion frameworks, namely, joint inversion of petrophysical coupled parameters and joint inversion of structurally coupled parameters. Joint inversion based on petrophysical coupled parameters introduces some prior rock physical property relationships into the inversion to improve the correlation between the physical properties [9], [11], [12]. Joint inversion based on structurally coupled parameters, however, seeks similar structure distributions between different physical properties [13], [14]. An example of the latter is the cross-gradient structure coupling method proposed by Gallardo and Meju [14], which has been widely recognized and adopted [6], [7], [10], [14]–[17].

For gravity and magnetic data, many scholars have developed 3-D joint inversion algorithms using structure coupling methods [18]–[21]. These methods mainly aim at improving the resolution of gravity and magnetic data, with less focus on computation efficiency and memory consumption. The 3-D gravity and magnetic joint inversion algorithm still uses traditional solving methods, such as least squares, Gauss–Newton (GN), and conjugate gradient (CG) methods. While the inversion resolution is improved, it is also necessary to optimize the calculation efficiency and memory consumption of the inversion. As such, lower computational cost algorithms suitable for 3-D gravity and magnetic joint inversion using structurally coupled parameters are desired.

Inspired by a 2-D data-space (DS) joint inversion in our previous study [10], we propose an improved 3-D DS joint inversion algorithm. In [10], we combined the DS method with the classical GN inversion method and applied it to the 2-D multiple parameter joint inversion. This can effectively reduce the dimension of the inversion iteration equation and improve the calculation efficiency and memory consumption of the joint inversion. However, this method needs to store the Jacobian matrix, which will consume a lot of memory for 3-D joint inversion. To avoid storing the Jacobian matrix, we introduce

Manuscript received February 10, 2021; revised April 1, 2021; accepted April 29, 2021. This work was supported in part by the National Key Research and Development Program of China under Grant 2017YFC0601606, in part by the China Postdoctoral Science Foundation Funded Project under Grant 2020TQ0114 and Grant 2020M681036, and in part by the Graduate Innovation Research Project of Jilin University under Grant 101832020CX227. *(Corresponding authors: Tonglin Li; Xingguo Huang.)*

Rongzhe Zhang, Tonglin Li, and Cai Liu are with the College of Geo-Exploration Sciences and Technology, Jilin University, Changchun 130026, China (e-mail: zhangrz@jlu.edu.cn; litl@jlu.edu.cn; liucai@jlu.edu.cn).

Xingguo Huang is with the College of Instrumentation and Electrical Engineering, Jilin University, Changchun 130012, China (e-mail: xingguohuang@jlu.edu.cn).

Kristian Jensen is with the Department of Earth Sciences, University of Bergen, 5020 Bergen, Norway (e-mail: kristian.jensen@uib.no).

Malte Sommer is with the GEOMAR Helmholtz Centre for Ocean Research Kiel, 24148 Kiel, Germany (e-mail: maltesommer@t-online.de).

Color versions of one or more figures in this letter are available at https://doi.org/10.1109/LGRS.2021.3077936.

Digital Object Identifier 10.1109/LGRS.2021.3077936

a truncated Gauss–Newton (TGN) method [22]–[24], which uses the CG method to approximately solve the GN iteration equation by a forcing term. By combining the DS and TGN methods, we present an algorithm referred to as DS-TGN and perform 3-D gravity and magnetic joint inversion by using the geometric trellis fast forward method [25] and the inexact structural resemblance (IESR) method [26] to further reduce the computational cost and memory consumption.

In the present work, we introduce the principle of joint inversion based on structurally coupled parameters in Section II. Next, in Section III, we present the DS-TGN algorithm used to solve the joint inversion objective function. In Sections IV and V, we present joint inversion results obtained from synthetic data and field data, respectively. Finally, Section VI provides the conclusion.

II. Structural Cross-Gradient Joint Inversion

There are usually two strategies for minimizing the cross-gradient function. One involves the use of the cross-gradient function as the equality constraint, added to the objective function by the Lagrange multiplier method to solve the minimization problem [6,] [10], [14], [17], [18], usually referred to as the exact structural resemblance method (ESR). The second strategy is to directly add the cross-gradient function to the objective function by a penalty term and minimize it [15], [16], [27], which is usually referred to as the IESR method. We choose to apply the IESR method mainly because it allows for flexible adding of prior structure information and it is easier to combine with different optimization algorithms [26].

The objective function for cross-gradient joint inversion of density and magnetic data is as follows:

$$\begin{aligned}\Phi(\mathbf{m}_1,\mathbf{m}_2)=&\sum_{i=1}^{2}(\mathbf{d}_i-\mathbf{f}_i(\mathbf{m}_i))^{\mathrm{T}}\mathbf{C}_{d_i}^{-1}(\mathbf{d}_i-\mathbf{f}_i(\mathbf{m}_i))\\&+\sum_{i=1}^{2}\lambda_i(\mathbf{m}_i-\mathbf{m}_{\mathrm{ir}})^{\mathrm{T}}\mathbf{C}_{m_i}^{-1}(\mathbf{m}_i-\mathbf{m}_{\mathrm{ir}})\\&+\beta_i\mathbf{t}^{\mathrm{T}}(\mathbf{m}_1,\mathbf{m}_2)\mathbf{t}(\mathbf{m}_1,\mathbf{m}_2)\end{aligned}\tag{1}$$

where $\mathbf{d}_i(i=1,\ 2)$ represent the gravity and magnetic data, and the corresponding model parameters $\mathbf{m}_i(i=1,\ 2)$ represent the density and magnetization, respectively. $\mathbf{m}_{\mathrm{ir}}(i=1,\ 2)$, respectively, represent the reference model of density and magnetization. $\mathbf{C}_{d_i}(i=1,\ 2)$ and $\mathbf{C}_{m_i}(i=1,\ 2)$ represent the data and model covariance matrices, respectively. The forward response of the gravity and magnetic method $\mathbf{f}_i(\mathbf{m}_i)$ $(i=1,\ 2)$ is a linear function, which can be expressed as $\mathbf{f}_i(\mathbf{m}_i)=\mathbf{A}_i\mathbf{m}_i$. $\mathbf{A}_i$ is the Jacobian matrix of the forward response. λ is the regularization factor, using the method in [28]. $\mathbf{t}$ is the cross-gradient function (see [18] for a derivation of its discrete form and partial derivative). β is the structural weighting factor, which is calculated by the ratio method.

In this letter, the gravity and magnetic forward adopts a fast method of geometric trellis. There is an equivalent relationship between the position of the model unit of the same layer and the observation point. It is only necessary to calculate the kernel function of the first model unit of each layer, and the kernel functions of other model units can be found through the equivalent relationship, thus improving the calculation efficiency. The model constraint term adopts the L_0-norm regularization term, which can handle sharp boundaries. The specific expression is

$$\Phi_m(\mathbf{m}_i)=\frac{1}{2}\ln\left(\mathbf{m}_i^2+\varepsilon^2\right).\tag{2}$$

We transform the model constraint term minimization problem into an iterative reweighted L_2-norm minimization problem, i.e., $\Phi_m(\mathbf{m}_i)=\|\mathbf{W}_{m_i}\mathbf{m}_i\|^2$. The model weighting matrix $\mathbf{W}_{m_i}$ can be expressed as

$$\mathbf{W}_{m_i}=\left(\frac{\partial\Phi_m(\mathbf{m}_i)}{\partial\mathbf{m}_i}\Big/\mathbf{m}_i\right)^{1/2}=\left(\mathbf{m}_i^2+\varepsilon^2\right)^{-1/2}.\tag{3}$$

The inversion result obtained by (1) will show anomalous bodies concentrated on the surface. This is because the kernel function of gravity and magnetic data attenuates with increasing depth, resulting in the skin effect of the inversion result. To improve the influence of the skin effect, a model integration sensitivity matrix, i.e., $\mathbf{S}_i=\mathrm{diag}(\mathbf{A}_i^{\mathrm{T}}\mathbf{A}_i)^{1/2}$ $(i=1,\ 2)$, is added to the model constraint. At this point, the model constraint can be rewritten as

$$\mathbf{C}_{m_i}^{-1}=\mathbf{S}_i^{\mathrm{T}}\mathbf{W}_{m_i}^{\mathrm{T}}\mathbf{W}_{m_i}\mathbf{S}_i.\tag{4}$$

For convenience, we integrate the model vectors, $\mathbf{m}=[\mathbf{m}_1;\mathbf{m}_2]$ and $\mathbf{d}=[\mathbf{d}_1;\mathbf{d}_2]$. The objective function of the $(k+1)$th iteration after integration is expressed as

$$\begin{aligned}\Phi(\mathbf{m}_{k+1})=&(\mathbf{d}-\mathbf{A}\mathbf{m}_{k+1})^{\mathrm{T}}\mathbf{C}_d^{-1}(\mathbf{d}-\mathbf{A}\mathbf{m}_{k+1})\\&+\lambda(\mathbf{m}_{k+1}-\mathbf{m}_{\mathrm{ref}})^{\mathrm{T}}\mathbf{C}_m^{-1}(\mathbf{m}_{k+1}-\mathbf{m}_{\mathrm{ref}})\\&+\beta\mathbf{t}(\mathbf{m}_{k+1})^{\mathrm{T}}\mathbf{t}(\mathbf{m}_{k+1})\end{aligned}\tag{5}$$

where $\mathbf{t}(\mathbf{m}_{k+1})\cong\mathbf{t}(\mathbf{m}_k)+\mathbf{B}_k(\mathbf{m}_{k+1}-\mathbf{m}_k)$ and $\mathbf{B}_k$ is the Jacobian matrix of the cross-gradient function.

III. Data-Space Truncated Gauss–Newton Method

The objective function in (5) is numerically solved by the GN method, and the expression of the model parameters $\mathbf{m}_{k+1}$ in the model space (MS) is as follows:

$$\begin{aligned}\mathbf{m}_{k+1}=\mathbf{m}_k+&\left(\mathbf{A}^{\mathrm{T}}\mathbf{C}_d^{-1}\mathbf{A}+\lambda\mathbf{C}_m^{-1}+\beta\mathbf{B}_k^{\mathrm{T}}\mathbf{B}_k\right)^{-1}\\&\times\left(\mathbf{A}^{\mathrm{T}}\mathbf{C}_d^{-1}\hat{\mathbf{d}}_k-\beta\mathbf{B}_k^{\mathrm{T}}\mathbf{t}(\mathbf{m}_k)\right)\end{aligned}\tag{6}$$

where $\hat{\mathbf{d}}_k=\mathbf{d}-\mathbf{A}\mathbf{m}_k$ and $\mathbf{m}_r=\mathbf{m}_k$.

In (6), the dimension of the inverted matrix of MS is $N_m\times N_m$, which is controlled by the size of the model parameter N_m. For actual 3-D problems, the number of model parameters is usually large, which makes it impractical to use the GN inversion method. To improve the computational efficiency of the GN method when solving the linear equations in (6), it is necessary to reduce the dimension of linear equations. This may be achieved by the DS method [29], [30], and the calculation of linear equations is transferred from the MS domain to the DS domain. Note that in [30], the iterative GN linear equations do not include the structural constraints in (6). The model update expression based on DS is as follows:

$$\begin{aligned}\Delta\mathbf{m}_{k+1}&=\left(\mathbf{A}^{\mathrm{T}}\mathbf{C}_d^{-1}\mathbf{A}+\lambda\mathbf{C}_m^{-1}\right)^{-1}\left(\mathbf{A}^{\mathrm{T}}\mathbf{C}_d^{-1}\hat{\mathbf{d}}_k\right)\\&=\mathbf{C}_m\left(\mathbf{A}^{\mathrm{T}}\mathbf{C}_d^{-1}\mathbf{A}\mathbf{C}_m+\lambda\mathbf{I}\right)^{-1}\left(\mathbf{A}^{-\mathrm{T}}\right)^{-1}\mathbf{C}_d^{-1}\hat{\mathbf{d}}_k\\&=\mathbf{C}_m\mathbf{A}^{\mathrm{T}}\left(\mathbf{A}\mathbf{C}_m\mathbf{A}^{\mathrm{T}}+\lambda\mathbf{C}_d\right)^{-1}\hat{\mathbf{d}}_k\end{aligned}\tag{7}$$

TABLE I

MAXIMUM MEMORY CONSUMPTION DURING THE CALCULATION OF DIFFERENT JOINT INVERSION METHODS

	30×30×30	50×50×50	100×100×100
DS-GN	1.328GB	11.845GB	>148GB
DS-GNCG	0.101GB	0.154GB	0.852GB
DS-TGN	0.101GB	0.154GB	0.852GB

where $\mathbf{I}$ is the identity matrix, $\mathbf{A}^{\mathrm{T}}\mathbf{C}_d^{-1}\mathbf{A}+\lambda\mathbf{C}_m^{-1}$ is a positive semidefinite symmetric matrix of size $N_m \times N_m$, and $\mathbf{A}\mathbf{C}_m\mathbf{A}^{\mathrm{T}}+\lambda\mathbf{C}_d$ is a positive semidefinite symmetric matrix of size $N_d \times N_d$. N_d is the number of data, and N_d is usually much smaller than N_m.

In [10], the model update expression for the joint inversion in the DS domain is given, but it is based on an ESR method to construct and calculate the 2-D objective function. The linear equations are then directly solved iteratively. We apply the IESR method instead to construct and calculate the 3-D objective function. Thus, we rederive the model update expression in the DS domain as follows:

$$\begin{aligned}\Delta\mathbf{m}_{k+1} &= \left(\mathbf{A}^{\mathrm{T}}\mathbf{C}_d^{-1}\mathbf{A}+\lambda\mathbf{C}_m^{-1}+\beta\mathbf{B}_k^{\mathrm{T}}\mathbf{B}_k\right)^{-1}\left(\mathbf{A}^{\mathrm{T}}\mathbf{C}_d^{-1}\hat{\mathbf{d}}_k-\beta\mathbf{B}_k^{\mathrm{T}}\mathbf{t}_k\right)\\ &= \mathbf{C}_k\mathbf{A}^{\mathrm{T}}\left(\mathbf{A}\mathbf{C}_k\mathbf{A}^{\mathrm{T}}+\mathbf{C}_d\right)^{-1}\hat{\boldsymbol{d}}_k\\ &\quad+\beta\mathbf{C}_k\mathbf{A}^{\mathrm{T}}\left(\mathbf{A}\mathbf{C}_k\mathbf{A}^{\mathrm{T}}+\mathbf{C}_d\right)^{-1}\mathbf{A}\mathbf{C}_k\mathbf{B}_k^{\mathrm{T}}\mathbf{t}_k-\beta\mathbf{C}_k\mathbf{B}_k^{\mathrm{T}}\mathbf{t}_k\\ &= \mathbf{C}_k\mathbf{A}^{\mathrm{T}}\left(\mathbf{R}_k^{-1}\mathbf{L}_k\right)-\beta\mathbf{C}_k\mathbf{B}_k^{\mathrm{T}}\mathbf{t}_k \qquad (8)\end{aligned}$$

where $\mathbf{C}_k=(\lambda\mathbf{C}_m^{-1}+\beta\mathbf{B}_k^{\mathrm{T}}\mathbf{B}_k)^{-1}$, $\mathbf{L}_k=\hat{\mathbf{d}}_k+\beta\mathbf{A}\mathbf{C}_k\mathbf{B}_k^{\mathrm{T}}\mathbf{t}_k$, and $\mathbf{R}_k=\mathbf{A}\mathbf{C}_k\mathbf{A}^{\mathrm{T}}+\mathbf{C}_d$.

We do not directly solve (8), because storing the Jacobian matrix requires a lot of memory space. Instead, we use a TGN method to solve (8). The TGN method combines the GN and CG methods. In each iteration, the CG method is used to approximately solve the GN iterative equations in order to obtain the model update. Using the CG method to solve the GN iterative equation requires dozens or hundreds of iterations. Although storing of the Jacobian matrix is avoided, it nevertheless takes a substantial amount of time to perform forward calculations repeatedly. In order to mitigate this, a forcing term is needed to control the accuracy of solving GN iteration equations. The choice of the forcing term directly affects convergence, efficiency, and robustness of the TGN method.

The DS-TGN method can be divided into two main iterative loops. The outer joint inversion loop computes $\mathbf{L}_k$, but not $\mathbf{R}_k$ and $\mathbf{A}$. The inner loop is used to minimize $\mathbf{R}_k\mathbf{x}=\mathbf{L}_k$ with the CG method. The solution process only needs to form the product $\mathbf{R}_k\mathbf{p}$ of the matrix vector, where $\mathbf{p}$ is an arbitrary DS vector, instead of actually forming the matrix $\mathbf{R}_k$, effectively avoiding the formation and storage of the Jacobian matrix $\mathbf{A}$, which only need to calculate $\mathbf{Ap}$ and $\mathbf{A}^{\mathrm{T}}\mathbf{q}$, and $\mathbf{p}$ and $\mathbf{q}$ are, respectively, N_{m}-dimensional sum and N_{d}-dimensional vector. Both of these two matrix-vector products can be calculated by solving a forward problem. The forcing term $\zeta=\min[0.05, 1/k, \mathrm{norm}(\mathbf{L}_k)]$ is used to control the solution accuracy of the inner loop [22]. When the relative residual error is less than the forcing term, the inner loop is terminated.

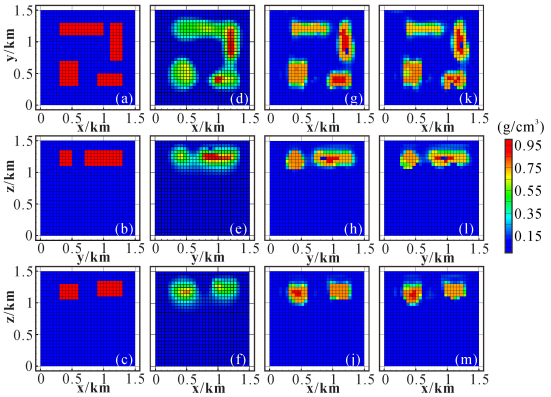

Fig. 1. (a)–(c) Slices of theoretical density models. Density models obtained by (d)–(f) separate inversion with DS-TGN. (g)–(i) Joint inversion with DS-GNCG. (k)–(m) Joint inversion with DS-TGN. The results are obtained for (a), (d), (g), and (k) $z=300$ m depth section, (b), (e), (h), and (l) $x=1200$ m cross section, and (c), (f), (j), and (m) $y=450$ m cross section.

IV. SYNTHETIC DATA EXAMPLE

In this section, we will compare the 3-D joint inversion results of gravity and magnetic data obtained via the DS Gauss–Newton method (DS-GN), the DS-GN conjugate gradient method (DS-GNCG), and the DS-TGN method in terms of memory consumption and resolution. We designed a model with four anomalous bodies of different mesh sizes in the MS. The three methods were used to perform joint inversion calculations on the models. The maximum memory consumption during joint inversion is shown in Table I. All computations were performed on an i7-8750H 2.21-GHz machine with 16 Gbyte of RAM. With an increase in the number of model meshes, the 3-D joint inversion obtained via the DS-GN method consumes significantly more memory, and ordinary computers can no longer meet the memory requirements. The memory consumption required for the DS-GNCG and DS-TGN methods, however, increases slowly, and even if the number of meshes reaches hundreds of thousands or even millions the computations can be performed on an ordinary computer.

In order to compare and analyze the resolution of the inversion results obtained from the DS-GNCG and DS-TGN methods, we present first the gravity and magnetic joint inversion results of model I ($30\times30\times30$). The physical properties, geometric sizes, and top burial depths of the anomalous bodies are shown in Figs. 1(a)–(c) and 2(a)–(c). The subsurface is discretized into $30\times30\times30$ prisms with a sampling size of 50 m in x-, y-, and z-directions. We use a homogeneous half-space model of 0 g/cm^3 and 0.001 A/m for the initial model. The initial regularization is $\lambda_1=10^{-2}$ and $\lambda_2=10^{-4}$.

The separate inversion results obtained by solving (7) using the TGN algorithm are shown in Figs. 1(d)–(f) and 2(d)–(f). The joint inversion results obtained from the DS-GNCG algorithm are shown in Figs. 1(d)–(f) and 2(d)–(f). This method uses the CG method to accurately solve the GN equation (residual typically must be set to less than 10^{-6}). The joint inversion results obtained from the DS-TGN algorithm are shown in Figs. 1(g)–(i) and 2(g)–(i). Fig. 3(a) and (b) shows the RMS value obtained throughout the iterations for both

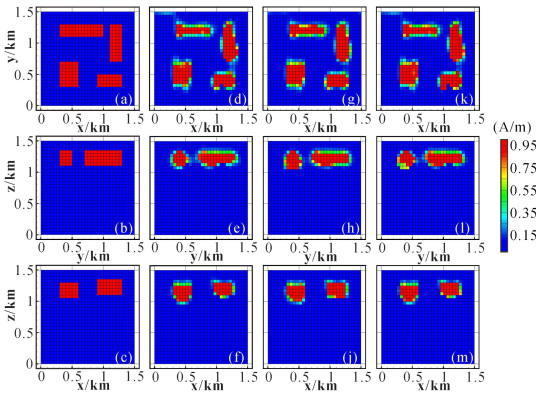

Fig. 2. (a)–(c) Slices of theoretical magnetization models. Magnetization models obtained by (d)–(f) separate inversion. (g)–(j) Joint inversion with DS-GNCG. (k)–(m) Joint inversion with DS-TGN. The results are obtained for (a), (d), (g), and (k) $z = 300$ m depth section, (b, (e), (h), and (l) $x = 1200$ m cross section, and (c), (f), (j), and (m) $y = 450$ m cross section.

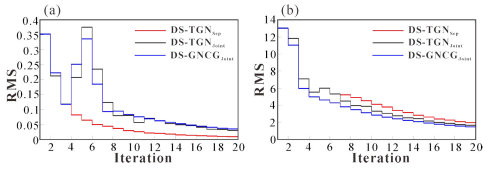

Fig. 3. Misfit curve for separate and joint inversion of (a) gravity data and (b) magnetic data.

examples. Note that the misfit of the inverted gravity data becomes larger in the fourth iteration, mainly because the algorithm starts the joint inversion calculation from the fourth iteration and only performs a separate inversion before in order to speed up the iteration convergence. The resolution of the magnetic separate inversion is higher than the gravity, so it will impose more structural constraints on the density model. The two joint inversion algorithms can obtain inversion results similar to the true model, whether in regard to the geometric shape of the anomalies or in terms of physical values, especially for the density model. Due to the addition of the model integration sensitivity matrix and the sparse constraint L_{0-} norm, we can retrieve sharp boundaries and eliminate the skin effect of the inversion results. For the synthetic case, the DS-GNCG algorithm required approximately 3.07 h, whereas the DS-TGN algorithm required approximately 0.93 h. This shows that the DS-TGN algorithm can meet the resolution requirements of 3-D gravity and magnetic data joint inversion, with smaller memory consumption and higher computational efficiency.

V. Real Data Example

To evaluate the practical applicability of the algorithm proposed in this letter, we apply the algorithm to field data obtained in the Huzhong area of Greater Khingan in northwestern Heilongjiang, China. The study area has frequent magma activities and is rich in mineral resources. The Yanshanian intermediate-acid magma intruded into the Jixianggou formation carbonate rock and produced contact metasomatism in its contact zone and interlayer structure, forming a skarn-type polymetallic deposit in the study area. For the detailed geological background, see [31]. The field measured data

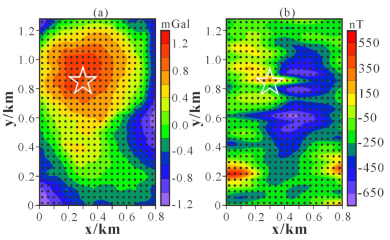

Fig. 4. (a) Gravity data and (b) magnetic data from a lead–zinc polymetallic deposit region in China. The black point is the observation point and the white five-pointed star is a known deposit area.

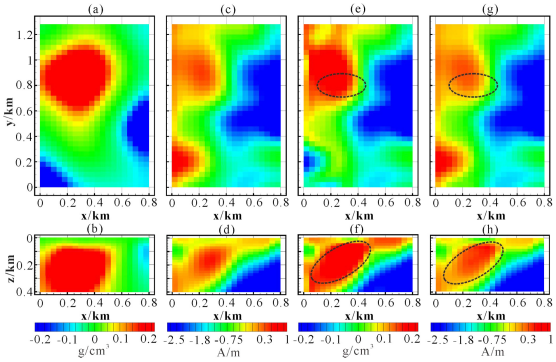

Fig. 5. (a) and (b) Slices of density model after separate inversion. (c) and (d) Magnetization model after separate inversion. (e) and (f) Density model after joint inversion. (g) and (h) Magnetization model after joint inversion. Slices (a), (c), (e), and (g) show the horizontal cross sections at $z = 260$ m. Slices (b), (d), (f), and (h) show the vertical cross sections at $y = 800$ m. The black dotted circle is the predicted deposit area.

include 640 gravity and 640 magnetic data (see Fig. 4). The point distance and line distance are 40 m. The inclination and declination values of the ambient field were about $I = 69.7°$ and $D = -11.35°$, respectively. We assume that there is only an inductive magnetization source.

For the inversion process, the underground space is divided into a cube of size $20 \times 32 \times 20$. All model cells were set to 0 g/cm^3 and 0.001 A/m for the starting model. Fig. 5 shows the results of a horizontal and a vertical cross section of the separate and joint inversion. We found that the density and magnetization models obtained from separate inversion [Fig. 5(a)–(d)] have great structural differences, which brings difficulties to comprehensive interpretation. In particular, the density model has a large area divergence problem, even if the sparse constraint is used. However, the joint inversion results [Fig. 5(e)–(h)] improve the structural similarity between the density and magnetization models. The density model obtains a sharp and clear structure distribution of underground by the contribution of the structural constraints of the magnetization model. Because the ore deposit in the study area is a skarn-type deposit, the deposit is produced by the contact between intrusive granodiorite and metamorphic rock, which has high magnetic and high-density anomalies. Through the joint inversion results, we seek high magnetic and high-density anomalous areas, which can delineate the distribution of skarn deposits in this area, as shown by the black dotted circle in Fig. 5(e)–(h). Comparing the known deposit location in Fig. 4, we can find that the inferred deposit is consistent with the real deposit area, further verifying that the algorithm in this letter can

accurately recover the underground density and magnetization distribution and has certain validity and practicability.

VI. Conclusion

Based on the DS joint inversion method, we have successfully developed a new DS-TGN joint inversion method. The method has been applied on gravity and magnetic datasets, including both synthetic data and real data obtained in the field. Numerical simulating tests indicate that with an increase in the number of model meshes, 3-D joint inversion performed via the DS-GN method consumed significantly more memory, and ordinary computers can no longer meet the memory requirements. However, the memory consumption of the DS-GNCG and DS-TGN methods increases slowly, thus allowing us to invert 3-D joint inversion of large gravity and magnetic datasets with a personal computer (PC) requiring only small memory consumption. In addition, the DS-TGN method requires less calculation time than the DS-GNCG method due to the added forcing term, which improves the calculation efficiency of the joint inversion. Real data example shows that the DS-TGN joint inversion method can obtain sharp, clear, and consistent structure density and magnetization models. According to the high-density and high magnetic anomalies in the joint inversion results, the location of skarn deposits can be accurately delineated. It further illustrates that the DS-TGN joint inversion method is an effective technical means for the exploration of skarn deposits, which can provide reference and guidance for the same type of deposits.

Acknowledgment

The authors would like to thank Bradley Weymer for his contribution to the revision of this letter.

References

[1] D. D. Jackson, "The use of a priori data to resolve non-uniqueness in linear inversion," *Geophys. J. Int.*, vol. 57, no. 1, pp. 137–157, Apr. 1979.

[2] Y. G. Li and D. W. Oldenburg, "3D inversion of magnetic data," *Geophysics*, vol. 61, no. 2, pp. 394–408, Mar. 1996.

[3] O. Portniaguine and M. S. Zhdanov, "Focusing geophysical inversion images," *Geophysics*, vol. 64, no. 3, pp. 874–887, May 1999.

[4] D. Fournier and D. W. Oldenburg, "Inversion using spatially variable mixed ℓ_p norms," *Geophys. J. Int.*, vol. 218, no. 1, pp. 268–282, Jul. 2019.

[5] T. Astic and D. W. Oldenburg, "A framework for petrophysically and geologically guided geophysical inversion using a dynamic Gaussian mixture model prior," *Geophys. J. Int.*, vol. 219, no. 3, pp. 1989–2012, Dec. 2019.

[6] L. A. Gallardo, "Joint two-dimensional DC resistivity and seismic travel time inversion with cross-gradients constraints," *J. Geophys. Res.*, vol. 109, no. B3, Mar. 2004, Art. no. B03311.

[7] W. Hu, A. Abubakar, and T. M. Habashy, "Joint electromagnetic and seismic inversion using structural constraints," *Geophysics*, vol. 74, no. 6, pp. R99–R109, Nov. 2009.

[8] H. Cai and M. S. Zhdanov, "Joint inversion of gravity and magnetotelluric data for the depth-to-basement estimation," *IEEE Geosci. Remote Sens. Lett.*, vol. 14, no. 8, pp. 1228–1232, Aug. 2017.

[9] B. Heincke, M. Jegen, M. Moorkamp, R. W. Hobbs, and J. Chen, "An adaptive coupling strategy for joint inversions that use petrophysical information as constraints," *J. Appl. Geophys.*, vol. 136, pp. 279–297, Jan. 2017.

[10] R. Z. Zhang, T. Li, X. Deng, X. Huang, and Y. Pak, "2D data-space joint inversion of MT, gravity, magnetic, and seismic data with cross-gradient constraints," *Geophys. Prospecting*, vol. 68, no. 2, pp. 721–731, Jan. 2020.

[11] O. Coutant, M. L. Bernard, F. Beauducel, F. Nicollin, M. P. Bouin, and S. Roussel, "Joint inversion of P-wave velocity and density, application to La Soufrière de guadeloupe hydrothermal system," *Geophys. J. Int.*, vol. 191, no. 2, pp. 723–742, Nov. 2012.

[12] J. Kamm, I. A. Lundin, M. Bastani, M. Sadeghi, and L. B. Pedersen, "Joint inversion of gravity, magnetic, and petrophysical data—A case study from a gabbro intrusion in Boden, Sweden," *Geophysics*, vol. 80, no. 5, pp. B131–B152, Sep. 2015.

[13] E. Haber and D. Oldenburg, "Joint inversion: A structural approach," *Inverse Problems*, vol. 13, no. 1, pp. 63–77, Feb. 1997.

[14] L. A. Gallardo and M. A. Meju, "Characterization of heterogeneous near-surface materials by joint 2D inversion of dc resistivity and seismic data," *Geophys. Res. Lett.*, vol. 30, no. 13, p. 1658, Jul. 2003.

[15] A. Tryggvason and N. Linde, "Local earthquake (LE) tomography with joint inversion for P-and S-wave velocities using structural constraints," *Geophys. Res. Lett.*, vol. 33, no. 7, Apr. 2006, Art. no. L07303.

[16] N. Linde, A. Tryggvason, J. E. Peterson, and S. S. Hubbard, "Joint inversion of crosshole radar and seismic traveltimes acquired at the south oyster bacterial transport site," *Geophysics*, vol. 73, no. 4, pp. G29–G37, Jul. 2008.

[17] R. Zhang, T. Li, S. Zhou, and X. Deng, "Joint MT and gravity inversion using structural constraints: A case study from the Linjiang copper mining area, Jilin, China," *Minerals*, vol. 9, no. 7, p. 407, Jul. 2019.

[18] E. Fregoso and L. A. Gallardo, "Cross-gradients joint 3D inversion with applications to gravity and magnetic data," *Geophysics*, vol. 74, no. 4, pp. L31–L42, Jul. 2009.

[19] F. Joulidehsar, A. Moradzadeh, and F. D. Ardejani, "An improved 3D joint inversion method of potential field data using cross-gradient constraint and LSQR method," *Pure Appl. Geophys.*, vol. 175, no. 12, pp. 4389–4409, Dec. 2018.

[20] M. S. Zhdanov, A. Gribenko, and G. Wilson, "Generalized joint inversion of multimodal geophysical data using Gramian constraints," *Geophys. Res. Lett.*, vol. 39, no. 9, May 2012, Art. no. L09301.

[21] J. Zhou, X. Meng, L. Guo, and S. Zhang, "Three-dimensional cross-gradient joint inversion of gravity and normalized magnetic source strength data in the presence of remanent magnetization," *J. Appl. Geophys.*, vol. 119, pp. 51–60, Aug. 2015.

[22] S. C. Eisenstat and H. F. Walker, "Choosing the forcing terms in an inexact Newton method," *SIAM J. Sci. Comput.*, vol. 17, no. 1, pp. 16–32, Jan. 1996.

[23] Y. Liu, J. Yang, B. Chi, and L. Dong, "An improved scattering-integral approach for frequency-domain full waveform inversion," *Geophys. J. Int.*, vol. 202, no. 3, pp. 1827–1842, Sep. 2015.

[24] A. Pidlisecky, E. Haber, and R. Knight, "RESINVM3D: A 3D resistivity inversion package," *Geophysics*, vol. 72, no. 2, pp. 1–10, Mar. 2007.

[25] C. L. Yao, T. Y. Hao, Z. N. Guan, and Y. W. Zhang, "High-speed computation and efficient storage in 3D gravity and magnetic inversion based on genetic algorithms," *Chin. J. Geophys.*, vol. 46, no. 2, pp. 253–258, Mar. 2003.

[26] L. A. Gallardo and M. A. Meju, "Structure-coupled multiphysics imaging in geophysical sciences," *Rev. Geophys.*, vol. 49, no. 1, Mar. 2011, Art. no. RG1003.

[27] D. Colombo and D. Rovetta, "Coupling strategies in multiparameter geophysical joint inversion," *Geophys. J. Int.*, vol. 215, no. 2, pp. 1171–1184, Aug. 2018.

[28] O. Portniaguine and M. S. Zhdanov, "3-D magnetic inversion with data compression and image focusing," *Geophysics*, vol. 67, no. 5, pp. 1532–1541, Sep. 2002.

[29] W. Siripunvaraporn and G. Egbert, "An efficient data-subspace inversion method for 2-D magnetotelluric data," *Geophysics*, vol. 65, no. 3, pp. 791–803, May 2000.

[30] W. Siripunvaraporn, G. Egbert, Y. Lenbury, and M. Uyeshima, "Three-dimensional magnetotelluric inversion: Data-space method," *Phys. Earth Planet. Interiors*, vol. 150, nos. 1–3, pp. 3–14, May 2005.

[31] S. P. Li *et al.*, "Application of 3D inversion of gravity magnetism electric method in upper mining area of Xiagalai Aoyi river," *Global Geol.*, vol. 39, no. 2, pp. 437–443, May 2020.